Check for updates

Freestanding electrodes with polyaniline/Au derived from electrospun carbon nanofibers for high-performance supercapacitors†

Yan Bu, Yunwei Zou, Ruibai Cang, Xuejiao Zhou,* Peng Yu [iD] and Mingyi Zhang [iD]*

Freestanding electrodes with the advantage of continuous conductive paths are more appealing for supercapacitor applications. In this work, using electrospun carbon nanofibers (CNFs) as conductive supports, Au nanoparticles (NPs) were embedded in polyaniline (PANI) polymer to construct a freestanding CNFs/PANI/Au electrode without binder. The binder-free CNFs/PANI/Au electrode with a meaningful three-dimensional (3D) network framework presents enhanced electrochemical properties. The specific capacitance of the CNFs/PANI/Au electrode (1144.5 F g^{-1}) was 2.69-fold that of CNFs/PANI, and was 5.85-fold that of CNFs/Au electrodes at a current density of 0.5 A g^{-1} in the three-electrode configuration, when the atomic weight of Au NPs was about 2.23 at%. The satisfactory capacitance properties were connected with the freestanding structure and the efficient charge transfer that occurs at the CNFs/PANI/Au heterojunction interface. Besides, benefiting from the unique 3D self-supporting nanostructures, the CNFs/PANI/Au electrode exhibits long-term cycling stability with about 86.5% specific capacitance retention at 2 A g^{-1} of initial capacitance after 5000 cycles. Our work provides a flexible strategy to construct freestanding and binder-free electrodes, which is expected to improve and optimize energy-storage devices.

1. Introduction

Freestanding electrodes are receiving increasing attention with the development of wearable and flexible electron devices.[1–3] Electrode materials are a vital part of freestanding electrodes and can directly influence the electrochemical performance of flexible devices.[4–6] Compared with transition metal oxides or hydroxide electrode materials, polyaniline (PANI) conductive polymer has been widely used in the manufacture of freestanding electrodes due to its low cost, superior flexibility, and satisfactory environmental stability.[7–10] Moreover, PANI has the intrinsic advantage of multiple redox states, which contributes to its high theoretical capacitance and excellent rate capability for pseudo-capacitors. However, the conductivity of PANI polymer is relatively low (approximately 11.9 S cm^{-1} for doped state in the presence of 1.2 M hydrochloric acid at 20 °C), making it challenging to meet the demand for high-capacity supercapacitors.[11–13] Embedding

metal NPs in the electrodes can significantly improve the conductivity of the PANI polymer.[14,15]

Among various metal NPs, Au NPs have been widely considered because of their excellent electrical conductivity of about 1.0×10^5 S m^{-1} and environmental stability, which may effectively prevent the degradation of acidic or alkaline electrolytes during the charge/discharge process.[16–18] Hence, the embedding of nano-scale Au NPs into amorphous PANI not only boosts the electrical characteristics of PANI nanostructures, but it also efficiently increases charge transfer efficiency between the surfaces of the PANI/Au hybrid electrode.[19–21] Regrettably, in the charge/discharge process, the irregular nanostructures and larger aggregations of PANI/Au hybrid significantly impair the kinetics and utilization efficiency of electrodes.[11,16] Moreover, the volume of PANI may alter the ion extraction or insertion during the charge–discharge cycles, causing the structural destruction and further limiting the application of the PANI/Au hybrid electrode for supercapacitors.[22,23] Besides, the majority of PANI/Au or PANI-based electrodes must be coated on the active materials using a conductive adhesive during the manufacture of supercapacitor electrodes.[24–26] However, the uneven contact that occurs during the mechanical mixing of carbon black, active materials, and polymer binders (like polyvinylidene difluoride or polytetrafluoroethylene) in the conventional slurry-derived electrode preparation process inevitably leads to the formation of "dead surfaces" or "dead volumes".[22,27] Additionally, the

Key Laboratory for Photonic and Electronic Bandgap Materials, Ministry of Education, School of Physics and Electronic Engineering, Harbin Normal University, Harbin 150025, People's Republic of China.
E-mail: zhouxj@hrbnu.edu.cn, zhangmingyi@hrbnu.edu.cn; Tel: +86 45188060349

† Electronic supplementary information (ESI) available: Histograms of the diameter of CNFs, CNFs/PANI, CNFs/Au, and CNFs/PANI/Au nanofiber electrodes, as well as CV and GCD curves of the CNFs, CNFs/PANI, and CNFs/Au nanofibers, are displayed in the ESI. See DOI: https://doi.org/10.1039/d4ce00625a

microstructures of the active materials are easily damaged during the grinding or ultrasonic treatment process used to make the electrode slurry. The ion-transport kinetics is greatly slowed down by the collapsed structures, which in turn influences the capacitive characteristics of electrode materials.

Based on the above issues, it is worthwhile to create binder-free electrodes with self-supporting structures by loading PANI/Au nanostructures onto appropriate supports. As is known, electrospun carbon nanofibers (CNFs) are a viable substrate for energy storage systems due to their mechanical strength, flexibility, and high conductivity, which ranges from 10^{-7} to 10^{-5} Ω m.[28–31] Also, CNFs with ultralong one-dimensional structures can build three-dimensional (3D) network structures by cross-linking with one another during the electrospinning process, and are optimal supports for constructing freestanding electrodes.[32–35] Therefore, using CNFs as conductive supports to construct binder-free CNFs/PANI/Au nanostructures could alleviate the aforesaid challenges. The freestanding CNFs/PANI/Au electrode could not only prevent the addition of polymer binder, but also simplify the preparation procedure of supercapacitor electrodes. Meanwhile, binder-free electrodes with continuous conducting substrates could efficiently minimize internal resistance, resulting in improved electron and charge transport during the charge/discharge process.

Herein, the binder-free CNFs/PANI/Au electrode was obtained through the hierarchical assembly of PANI nanostructures and Au NPs on CNFs supports. The CNFs/PANI/Au electrodes with cross-linked 3D network structures are useful to increase the contact area of the electrode–electrolyte interface. The capacitive properties also improve significantly with the increase of ion diffusion rate. Besides, as an effective electron conduction bridge, Au NPs may be more useful in building high-efficiency electron transport channels at the heterojunction interface in CNFs/PANI/Au electrodes, which was favorable for improving the interfacial charge transfer rate of the CNFs/PANI/Au electrode. As expected, at 0.5 A g^{-1} current density, the binder-free and freestanding CNFs/PANI/Au electrode with a specific capacitance of 1144.5 F g^{-1} outperformed the CNFs/PANI (425 F g^{-1}) and CNFs/Au (195.5 F g^{-1}) electrodes significantly. Our findings suggest new approaches to promote the development of binder-free and freestanding electrodes in solid-state supercapacitors and flexible electronic devices.

2. Experiment

2.1. Materials

Polyacrylonitrile (PAN, ~99.0%) with a molecular weight of approximately 150 000, aniline ($C_6H_5NH_2$, ~99.5%), and tetrachloroauric acid tetrahydrate ($HAuCl_4 \cdot 4H_2O$, ≥47.8%) were produced by Sigma-Aldrich Corporation. Ferric chloride hexahydrate ($FeCl_3 \cdot 6H_2O$, ~99.0%), stannous chloride ($SnCl_2 \cdot H_2O$, ~98.0%), and N,N-dimethylformamide (DMF, ~99.5%) were made by Tianjin Zhiyuan Corporation. The laboratory manager purchased hydrochloric acid (HCl, 36.0–38.0%), concentrated nitrate (HNO_3, 65.0–68.0%), and ammonium hydroxide ($NH_3 \cdot H_2O$, 25.0–28.0%) reagents from Kermel Analytical Reagent Company.

2.2. Preparation of the CNFs/PANI nanofiber electrode

The CNFs substrates could be obtained by calcination of electrospun PAN nanofibers at 900 °C in argon shielding gas.[36,37] The CNFs were submerged in nitric acid for 48 hours, and then rinsed with deionized water until the filtrate had a pH of 7. The uniform PANI nanostructures were grown on CNFs by *in situ* chemical polymerization of aniline monomers. In a typical synthetic approach, the as-prepared CNFs (20 mg) were put in a 30 mL mixed solution of ferric chloride (9 mmol) and HCl solution (6 mmol). Moreover, 4.5 mmol of aniline monomer was gradually added to the aforementioned combination. The mixed solution was maintained at 60 °C for approximately 12 hours. The CNFs/PANI nanofibers were generated by repeating the above-mentioned method five times. The CNFs/PANI nanofibers were then produced by washing with ethanol and ultrapure water alternately. The final products of CNFs/PANI nanofibers were obtained by drying at low temperature.

2.3. Synthesis of the CNFs/PANI/Au nanofiber electrode

Au NPs were *in situ* immobilized on the CNFs/PANI nanofibers *via* a facile redox process, as previously studied.[38] The preparation process of CNFs/PANI/Au nanofibers is shown in Scheme 1. The as-prepared CNFs/PANI nanofibers (20 mg) were immersed in a $SnCl_2$ solution (0.25 M; 20 mL) under magnetic stirring for 12 hours. Then, the activated CNFs/PANI nanofibers were added into a mixed solution of $HAuCl_4$ (0.12 M; 20 μL) and ammonium hydroxide (8.4 M; 10 mL), and stirred for 25 minutes. Notably, ammonia was utilized to efficiently control the size of Au NPs and avoid the formation of large-sized Au aggregates on the surface of the CNFs/PANI nanofibers, according to the relevant literature.[39,40] The washing and drying of CNFs/PANI/Au nanofiber electrodes were the same as those of CNFs/PANI nanofibers.
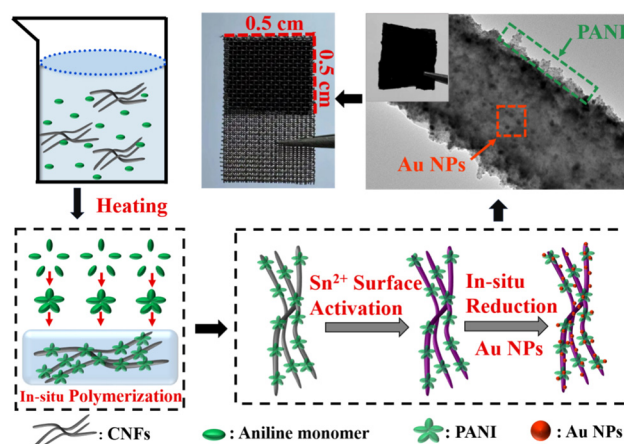
Scheme 1 Graphical synthetic routes of freestanding the CNFs/PANI/Au electrode.

For contrast, the CNFs/Au nanofibers were also prepared by growing Au particles directly on CNFs under identical conditions.

2.4. Characterization

Scanning electron microscopy (SEM, Hitachi-SU70), transmission electron microscopy (TEM, PHILIPS TECNAI-20), and X-ray diffraction (XRD, D/max2600) from Rigaku were applied to detect and analyze the microstructures of the as-prepared electrodes. The ALPHA infrared spectrometer was used to detect the bonding of samples by Fourier transform infrared spectroscopy (FTIR) analysis. Additionally, the instrument model AXIS SUPRA+ (Shimadzu, Japan) was devoted to measure the X-ray photoelectron spectroscopy (XPS) data of electrode materials.

2.5. Electrochemical measurements

The CNFs/PANI/Au nanofiber electrode was investigated in 1 M H_2SO_4 electrolyte using a standard three-electrode setup. A platinum foil electrode and a silver chloride electrode were used as the counter electrode and reference electrode, respectively. Notably, the CNFs/PANI/Au nanofibers were squeezed between two stainless steel meshes, resulting in a working electrode weighing approximately 0.8 mg. The binder-free and freestanding electrodes prepared under 3 MPa pressure have an area of approximately 0.5×0.5 cm^2 and a thickness of approximately 40 μm. Scheme 1 shows the physical picture of the CNFs/PANI/Au nanofiber electrode. The as-fabricated CNFs/PANI/Au nanofiber electrode demonstrated a macroscopic lamellated structure, allowing tweezers to pick up the fibrous membranes. The self-supporting structure of the CNFs/PANI/Au electrode allows for the creation of new-style integrated electrodes that do not require any conductive adhesives. The electrochemical characteristics of the obtained electrodes were measured using an electrochemical workstation (VMP3, France). Electrochemical impedance spectroscopy (EIS) was carried out using an interference amplitude of 5 mV. Cyclic voltammetry (CV) processes achieved series scanning speeds of 5, 10, 20, 30, 50, and 100 mV s^{-1} at an appropriate voltage interval of −0.2 ~0.8 V. In the corresponding voltage range, the current densities of galvanostatic charge/discharge (GCD) processes increase from 0.5 to 8 A g^{-1}, respectively. The specific capacitance value of the electrode was calculated using eqn (1). The formula denotes the specific capacitance (F g^{-1}) as Cm; the response current as I (A); and the discharge time (s), active material mass (g), and voltage interval (V) as Δt, m, and ΔV, respectively.

$$Cm = \frac{I \times \Delta t}{m \times \Delta V} \tag{1}$$

3. Results and discussion

The microstructures of the electrode materials were examined using SEM and TEM images. The CNFs exhibited a smooth surface with an average diameter of around 158.3 nm (Fig. 1a and S1a†). The continuous spiny PANI polymers were uniformly grafted onto the surface of the CNF by *in situ* polymerization of aniline molecules (Fig. 1b). The attached spinous and corrugated PANI revealed the large specific surface area of CNF/PANI nanofibers, making it easier to trap Au NPs on their surface during the synthesis processes. In comparison to CNF/PANI, SEM images of CNFs/PANI/Au and CNFs/Au nanofibers revealed many nanometer-sized Au NPs with spherical shapes (Fig. 1c and d). In addition, CNFs/PANI nanofibers (~488.7 nm) and CNF/PANI/Au nanofibers (~499.5 nm) have significantly greater diameters compared to CNFs and CNF/Au nanofibers (Fig. S1b–d†). Meanwhile the CNFs/PANI/Au nanofibers retain a stable 3D network structure developed from CNFs. This contributes to optimizing the free-standing properties of the nanofiber electrodes.

Fig. 1e shows a TEM image of a CNFs/PANI/Au nanofiber with a one-dimensional nanostructure consisting of homogeneous PANI polymeric layers and highly distributed Au NPs. CNFs supports with a high surface area provide abundant active centers, facilitating intimate interaction with both PANI and Au NPs. Also, the agglomeration of aniline monomer may be avoided during the *in situ* polymerization process. Notably, a portion of Au NPs were incorporated in the PANI polymer matrix to generate a particular coating heterostructure (Fig. 1e inset). The lattice stripe spacing of the Au NPs is 0.236 nm, corresponding to the (1 1 1) lattice plane in the HRTEM image (Fig. 1f).[16] In addition, the contrast between the PANI polymer and the dark Au NPs clearly distinguishes the heterostructure, which improves the
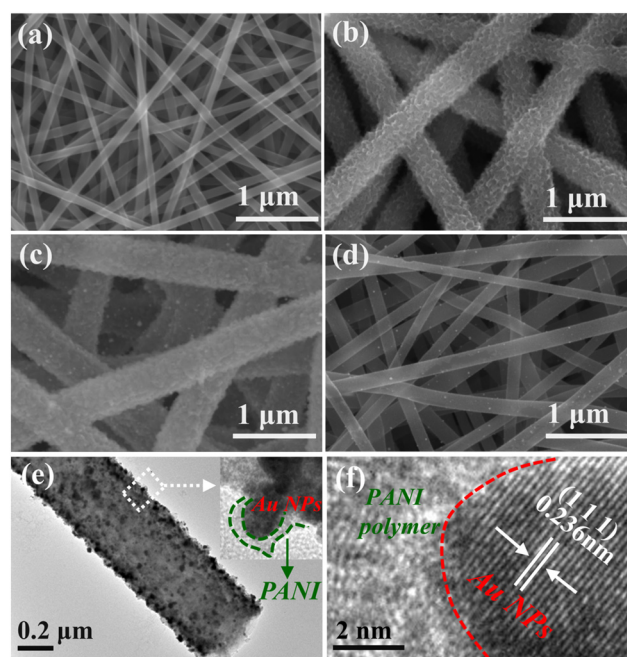

Fig. 1 SEM images of (a) CNFs, (b) CNFs/PANI, (c) CNFs/PANI/Au and (d) CNFs/Au nanofibers; (e) TEM and (f) HRTEM images of the CNFs/PANI/Au nanofibers.

stability of the hybrid structure and promotes charge transfer at the heterojunction interface between PANI and Au NPs.

Fig. 2a shows the XRD spectrogram, where all the samples have the usual broad peak of CNFs at $2\theta \sim 24.1°$. The typical characteristic peaks of PANI at 15° and 25° were observed in the CNFs/PANI and CNFs/PANI/Au nanofibers. Four characteristic peaks were observed clearly in the samples of CNFs/PANI/Au and CNFs/Au nanofibers at 38.2°, 44.4°, 64.6°, and 77.5°, which was attributed to the (1 1 1), (2 0 0), (2 2 0), and (3 1 1) crystal planes of Au NPs (JCPDS no. 040784), respectively.[4,16] In addition, the content of the Au element in CNFs/PANI/Au (2.23 at%) and CNFs/Au (2.54 at%) nanofibers was virtually the same during the simultaneous synthesis process of Au NPs, according to the EDX data (Table 1). These results confirm that Au NPs with good crystallinity and controllable loading capacity can be successfully assembled on CNFs/PANI/Au nanofibers.

The chemical bonding and structures of the as-prepared nanofiber electrodes were further analyzed using FTIR spectra (Fig. 2b). The absorption peaks of CNFs and CNFs/Au nanofibers at 804 and 1579 cm^{-1} result from the bending vibration of C–H and the stretching vibrations of COO– groups, respectively.[4,41] Also, the characteristic bands of the C–H stretching vibration appear in the wave-number interval of 2800 $\sim$3000 cm^{-1}.[42,43] For the spectra of CNFs/PANI nanofibers, the peaks at 1565 and 1485 cm^{-1} are derived from the C=C stretching vibration.[44] The C–N bond of the secondary aromatic amine appears at 1286 cm^{-1}.[44] PANI showed two bonds of C–N$^+$– and N–H$^+$ at 1170 and 1103 cm^{-1}, respectively.[16] The plane stretching of C–H and –NH– characteristic bonds were shown in wavenumbers of 820 and 3221 cm^{-1}. Notably, the C–H, C–N$^+$–, and C=C bonds of CNFs/PANI/Au nanofibers were significantly shifted at 834, 1157 and 1578 cm^{-1}, respectively.[45] This result indicated the effective interaction between Au NPs and the PANI matrix. The strong interaction on the CNFs/PANI/Au nanofibers may promote the stability of the heterojunction and assist the effective transfer of interfacial charge for charge storage operation.

The XPS full-spectrum of CNFs/PANI/Au nanofiber electrode demonstrated the existence of the Au element as shown in Fig. 2c. The residual Sn originates from the stannous chloride reducing agent remaining from the *in situ* reduction process of Au NPs. The Au 4f spectrum of the CNFs/PANI/Au nanofiber electrode has two typical peaks at 83.7 and 87.4 eV, separately (Fig. 2f).[46,47] The photoelectron peak with binding energy at 284.6 eV is attributed to the C–C bond of CNFs (Fig. 2d and g). The binding energy at 285.9 eV originates from the C–O group. The N–C=N bond at 287.4 eV is from the quinone-like structure of the PANI polymer component over the CNFs/PANI nanofiber electrode.[36] Also, the peak binding energies of the N 1s spectra at 398.9, 400.6, and 402.5 eV over the CNFs/PANI nanofiber electrode come from the typical quinoid amine (–N=), benzenoid amine (–NH–) and nitrogen cation radical (N$^+$), respectively (Fig. 2e).[29] Notably, the binding energy in the C–C bond of CNFs/PANI/Au nanofiber is shifted markedly to a higher binding energy (288.4 eV) as shown in Fig. 2g. Moreover, the above binding energies of N 1s on the CNFs/PANI/Au nanofiber electrode also reached the higher binding energies of 399.4, 402.4, and 404.4 eV, respectively (Fig. 2h). The shift of binding energies may be connected with the efficient formation of the PANI/Au heterojunction when the PANI component is in close contact with Au NPs.[48,49] Electrons are able to transfer spontaneously from PANI to the Au NPs with a high work-function of 5.1 eV.[48,50] The depletion of electrons on the PANI surface would result in a positive charge zone near the PANI component, which will increase the corresponding binding energies for the XPS test. Combined with the results of FTIR spectroscopy and TEM, Au NPs should act as electron acceptors to accelerate the charge transfer on the CNFs/PANI/Au nanofiber electrode at the component interface between PANI and Au NPs. Thus, the effective charge transfer behavior occurring on the CNFs/PANI/Au nanofiber electrode may greatly improve its electrochemical performance.

The charge storage performance of nanofiber electrodes was estimated with CV and GCD curves. Fig. 3a presents CV curves of the as-fabricated nanofiber electrodes with a slow-speed scanning of 5 mV s^{-1}. The CNFs/PANI and CNFs/PANI/Au nanofiber electrodes exhibited two groups of typical peaks in the CV curves, which can be ascribed to the redox transition of PANI between a semiconducting state (leucoemeraldine form) and a conducting state (polaronic emeraldine form) as well as the faradaic transformation of emeraldine pernigraniline, respectively.[44] There is no polarization observed in the CV data of the CNFs/PANI/Au electrode. This indicates that nanofiber electrodes with a 3D network
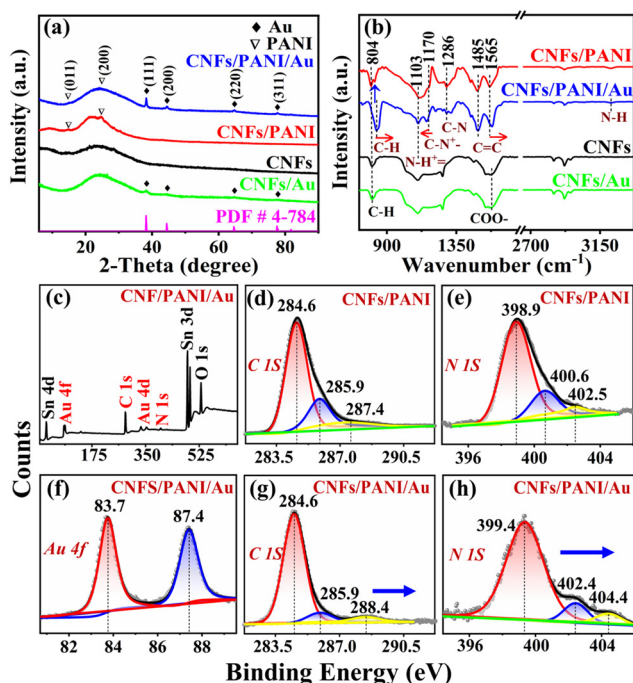

Fig. 2 (a) XRD diagrams and (b) FT-IR spectra of the as-fabricated samples; (c) survey XPS spectrum of CNFs/PANI/Au nanofibers, and XPS data of (d) C 1s and (e) N 1s core-level spectra for the CNFs/PANI nanofibers; XPS patterns of (f) Au 4f, (g) C 1s, and (h) N 1s core-level spectra for the CNFs/PANI nanofibers.

**Table 1** Experimental parameters and the EDX data of the electrode materials

Samples	Experimental conditions				Element contents		
	$FeCl_3 \cdot 6H_2O$ (g)	HCl (mL)	C_6H_7N (mL)	$HAuCl_4$ (μL)	C	N	Au (at%)
CNFs	—	—	—	—	87.48	12.52	—
CNFs/PANI	1.0	0.5	0.4	—	83.38	16.62	—
CNFs/PANI/Au	1.0	0.5	0.4	20	83.92	13.85	2.23
CNFs/Au	—	—	—	20	84.87	12.60	2.54

structure can be fully and efficiently utilized by the electrolyte and are more conducive to ion diffusion. Obviously, the integrated area of the CV curve of the CNFs/PANI/Au nanofiber electrode is larger than that of the CNFs/PANI electrode, indicating enhanced specific capacitance. The specific capacitance of the as-obtained samples was obtained according to eqn (1) in the GCD measurement with 0.5 A g^{-1} current density. To investigate the benefits of the freestanding CNFs/PANI/Au electrode, the electrode slurry of CNFs/PANI/Au was made by combining the active material, carbon black, and PVDF in an 8:1:1 ratio. The resulting mixture was then coated onto a stainless steel mesh for GCD testing. The specific capacitance of the slurry-coating CNFs/PANI/Au electrode is 423.9 F g^{-1} (Fig. S2a†) at a current density of 0.5 A g^{-1}, which is much less than that of the non-adhesive freestanding CNFs/PANI/Au electrode (1144.5 F g^{-1}), as shown in Fig. 3b. The structure and morphology of the CNFs/PANI/Au nanofibers are clearly disrupted throughout the process of manufacturing electrode slurry, as can be seen from the SEM following the GCD test (Fig. S2b†). This has a negative impact on the electrochemical performance of the slurry-coating CNFs/PANI/Au electrode. More importantly, the specific capacitance of CNFs/PANI/Au (1144.5 F g^{-1}) was significantly greater than that of CNFs/PANI (425.0 F g^{-1}), CNFs/Au (195.5 F g^{-1}), and CNFs (44.0 F g^{-1}), respectively (Fig. 3b). These results may be due to the contribution of Au

NPs, which promote faster and more effective electron transfer between the CNFs supports and the active components of PANI.

The enhanced capacitance performance of the as-obtained nanofiber electrodes was further investigated by cyclic voltammetry in H_2SO_4 electrolyte with the scanning rate increasing to 100 mV s^{-1}, as illustrated in Fig. 3c, S3a, c, and e.† The CNFs/PANI/Au and CNFs/PANI nanofiber electrodes showed an increased current density with increasing scan rate, demonstrating ideal capacitor behavior. Also, the potential of the redox peaks shifted in the direction of positive/negative potential as the scanning rate increased. This phenomenon indicates that a surface-controlled process of electrochemical polarization occurred at the electrode surface; similar results have been observed in the literature.[4,17] Besides, despite an increase in sweep speed, electrolyte ions still have difficulty reaching the bulk phase of the electrode material.[51] To improve the response kinetics during charge storage, modifying the electrode surface with Au NPs is an effective way to reduce the charge transfer resistance at the electrode–electrolyte interface. As shown in Fig. 3b, S3b, d, and f,† the GCD curves of CNFs/PANI/Au and CNFs/PANI nanofiber electrodes exhibited a nonlinear relation between potential and time, which was contributed by the CNFs-derived double-layer capacitance and the pseudo-capacitance behavior of the polyaniline substrate.[10,23]

Notably, the CNFs/PANI/Au and CNFs/PANI nanofiber electrodes retained 61.7 and 60.0% of the capacitance values at a higher ampere density of 8 A g^{-1} versus 1 A g^{-1}, as pictured in Fig. 4a. However, CNFs/Au and CNFs electrodes retained only 38.6 and 24.2% of their specific capacitance, respectively. It was determined that the spinous and corrugated structures of the PANI matrix on the CNFs surface may provide abundant active sites for the electrochemical process, hence increasing the rate capability of the electrodes noticeably. In particular, the capacitance value of the CNFs/PANI/Au nanofiber electrode at 0.5 A g^{-1} (1144.5 F g^{-1}) was actually 3.1 times that at 1 A g^{-1} (372 F g^{-1}) as shown in Fig. 4b. Based on the TEM image in the inset of Fig. 1e, it is likely that the PANI/Au heterojunctions formed on the CNFs/PANI/Au nanofiber electrodes. The unique heterostructure of these nanofiber electrodes helps the internal electrode material participate more fully in the electrochemical reaction at lower current densities.[11,16] Au NPs coated with the thin PANI nanostructures may decrease the charge transfer space between the Au NPs and PANI component, considerably increasing the charge transfer efficiency of
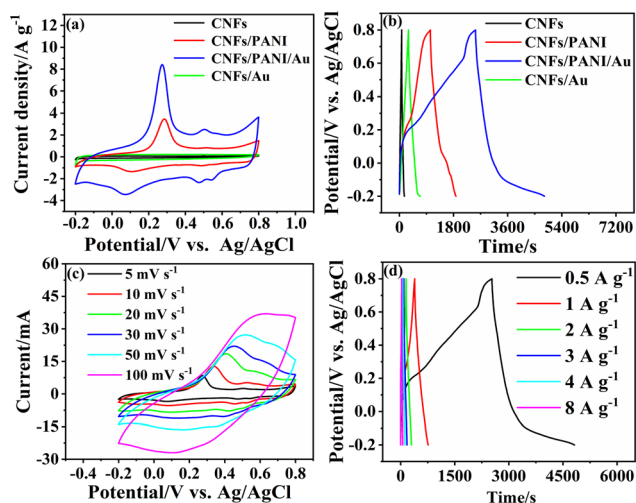
Fig. 3 (a) CV curves of nanofiber electrodes at 5 mV s^{-1}; (b) GCD curves of electrodes at 0.5 A g^{-1}; (c) CV and (d) GCD curves of the CNFs/PANI/Au nanofiber electrodes under different measurement conditions.
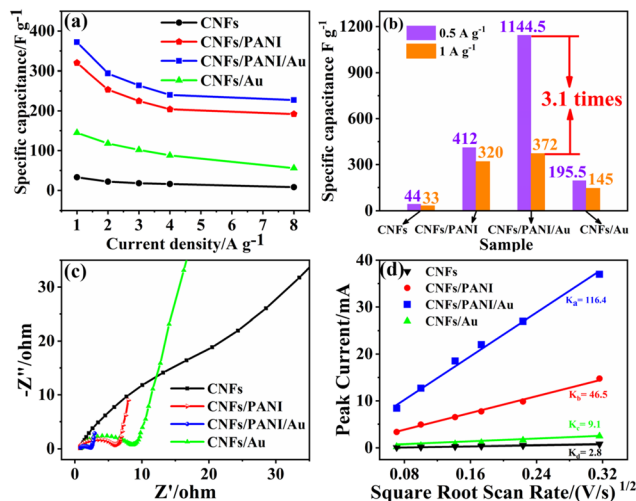
Fig. 4 (a) Capacitance values of the CNFs, CNFs/PANI, CNFs/PANI/Au and CNFs/Au nanofibers with multiple current densities; (b) the contrast diagram of capacitances for the samples at different current densities of 0.5 and 1 A g^{-1}; (c) Nyquist plots and (d) the linear relationship of the peak current *vs.* square root of scan rates for the as-obtained electrodes.

electrode materials. Also, the overall conductivity of the CNFs/PANI/Au nanofiber electrode will also be improved due to the participation of Au NPs in the PANI matrix. Furthermore, the capacitance values of the CNFs/PANI/Au nanofibers are very competitive compared to other similar electrode materials reported in the literature (Table 2). Based on the above analysis, the higher specific capacitance of the fabricated CNFs/PANI/Au nanofiber electrodes can be attributed to the synergistic action of their unique heterostructures and good charge transfer properties.

The charge transfer properties of nanofiber electrodes were evaluated by EIS analysis. The Nyquist spectra of the as-obtained nanofiber electrodes all exhibit a normal semicircle in the high-frequency section (Fig. 4c). The CNFs/PANI/Au nanofiber electrode shows a smaller diameter of the hemicircular arc compared to the CNFs/PANI, CNFs, and CNFs/Au nanofiber electrodes, which reflects a smaller charge-transfer resistance (R_{ct}). Besides, the CNFs/PANI/Au nanofiber electrode exhibits a straight line with an approximate vertical *Y*-axis in the low-frequency section. These results indicate that the contribution of Au NPs may promote high-efficiency charge/ion transfer at the electrode/electrolyte interfaces. The *K* values of ion diffusion rates were calculated using the classical Randles–Sevcik eqn (2).[51]

$$I_{\mathrm{p}} = (2.69 \times 10^5) n^{3/2} A D^{1/2} C_0 \nu^{1/2} \qquad (2)$$

The number of electrons transferred in the REDOX reaction is expressed as "*n*". *A* represents the active electrode area, C_0 indicates the mole concentration of the active substance involved in the redox reaction, and *D* represents the ion diffusion coefficient, respectively. The *K* value can be fitted from the linear relationship between the anodic peak current (I_{p}) and square root of the scan rates ($\nu^{1/2}$). According to eqn (2), the *K* value of the CNFs/PANI/Au nanofiber electrodes ($K_{\mathrm{a}} \sim 116.4$) was significantly higher than that of the CNFs/PANI ($K_{\mathrm{b}} \sim 46.5$), CNFs/Au ($K_{\mathrm{c}} \sim 9.1$) and CNFs ($K_{\mathrm{d}} \sim 2.8$) electrodes as shown in Fig. 4d. This indicates that the CNFs/PANI/Au nanofiber electrodes with a unique heterostructure appeared to be more marketable than the other electrodes in the ion transport process.

Table 2 Capacitance values and cycling ability of the CNFs/PANI/Au nanofiber electrode contrast of relevant reports

Electrode material	Electrolyte	Specific capacitance	Cycle life	Ref.
PANI/N-CNFs electrode	1 M H_2SO_4	580.9 F g^{-1} (at 0.5 A g^{-1})	109.7% (90 000th at 20 A g^{-1})	31
PANI/CNFs electrode	1 M H_2SO_4	296.3 F g^{-1} (at 1 A g^{-1})	83.8% (2000th at 2 A g^{-1})	12
PANI/PSS/CNP electrode	1 M HCl	2.56 F cm^2 (at 2 mA cm^{-2})	81.5% (8000th at 10 mA cm^{-2})	2
PANI/CNFs/CNS electrode	1 M H_2SO_4	381.8 F g^{-1} (at 1 A g^{-1})	— —	30
PANI/GO/CNFs electrode	1 M H_2SO_4	680.8 F g^{-1} (at 0.5 A g^{-1})	93.5% (3000th at 3 A g^{-1})	29
PANI/CNFs/CNT electrode	1 M H_2SO_4	629.1 F g^{-1} (at 0.5 A g^{-1})	88.5% (5000th at 10 A g^{-1})	5
PANI/CNFs/MnO$_2$ electrode	1 M Na_2SO_4	654 F g^{-1} (at 10 mV s^{-1})	88.8% (1000th at 10 A g^{-1})	28
PANI/CNFs electrode	1 M H_2SO_4	493.75 F g^{-1} (at 1 mA cm^{-2})	90.0% (5000th at 1 mA cm^{-2})	52
rGO/PANI–Au electrode	0.5 M H_2SO_4	309 F g^{-1} (at 1 A g^{-1})	53.0% (2000th at 400 mV s^{-1})	53
rGO–Au@PANI electrode	1 M H_2SO_4	212.8 F g^{-1} (at 1 A g^{-1})	86.9% (5000th at 1 A g^{-1})	16
CNFs/PANI/Au electrode	1 M H_2SO_4	**1144.5 F g^{-1} (at 0.5 A g^{-1})**	**86.5% (5000th at 2 A g^{-1})**	**This work**

In this heterostructure system, the work function of Au was greater than CNFs (4.6 eV), leading them could act as electronic sinks to facilitate interfacial charge transfer between CNFs and Au NPs.[45] The known highest occupied molecular orbital (HOMO) of PANI (*vs.* NHE) is *ca.* +1.24 eV and the lowest unoccupied molecular orbital (LUMO) (*vs.* NHE) is *ca.* −1.11 eV.[54] The work function of the electrode materials can be calculated according to eqn (3).[48]

$$E \text{ (eV)} = E \text{ (V } vs. \text{ NHE)} + 4.5 \text{ V} \tag{3}$$

The computational work function of PANI is 3.39 eV. Such energy levels suggest that the electrons stored in the LUMO of PANI may diffuse to the surface of the CNFs and subsequently transfer to the Au NPs during the discharge process in path number 1 (Fig. 5). The depletion of electrons on the PANI surface would generate a positive charge space around the PANI component, resulting in a built-in electric field. Meanwhile, once Au NPs come into immediate contact with the PANI components, a portion of them construct PANI/Au core–shell structures as shown in the TEM images in Fig. 1e and f. As demonstrated in path number 2, the electrons of PANI may also be directly caught by the Au NPs, on account of the Schottky junction of Au/PANI that occurs in the CNFs/PANI/Au nanofiber electrode.[15,16,55] This multi-channel charge transfer path may promote the charge transfer efficiency, resulting in excellent capacitance retention during charge/discharge cycles.

The stability of the as-obtained nanofiber electrodes was examined in cycle testing with an ampere density of 2 A g^{-1} (Fig. 6a). The CNFs/PANI/Au nanofiber electrode retains approximately 86.5% of its initial capacitance after 5000 cycles, showing outstanding long-term cycling stability. Following cycle testing, the free-standing and binder-free electrode was disassembled, and it was found that the structures and morphologies of the CNFs/PANI/Au electrode remained mostly unchanged, as depicted in the SEM image in Fig. S4.† In addition, the 600th cycle saw a considerable rise in electrode capacitance, which could be attributed to the electrodes being
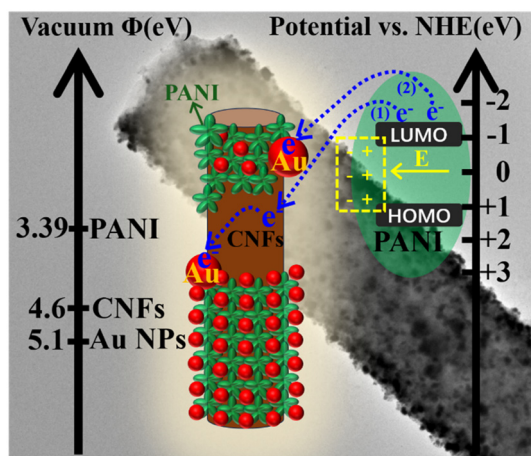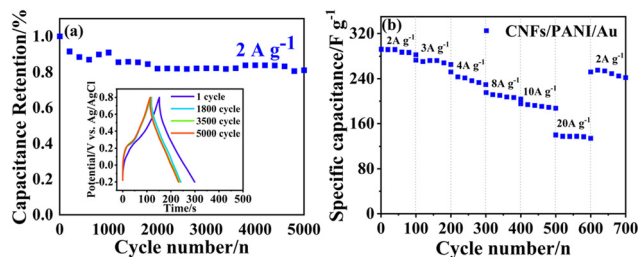

Fig. 6 (a) Cycling stability of the CNFs/PANI/Au nanofiber electrode for 5000 cycles, and the (inset) GCD curves of the CNFs/PANI/Au after the different cycle numbers; (b) rate capability of the CNFs/PANI/Au nanofiber electrode at the different current densities.

fully activated. The CNFs/PANI/Au nanofiber electrode presents a favorable repeatability of potential–time correlation after the different cycle numbers, respectively (Fig. 6a inset). The rate capacitance of the CNFs/PANI/Au nanofiber electrode was further investigated by cycle testing for 700 cycles with various high current densities from 2 to 20 A g^{-1} (Fig. 6b). The CNFs/PANI/Au nanofiber electrode exhibits outstanding rate capability performance. Even after the highest current density of 20 A g^{-1} cycle test, the invertible capacity (241.9 F g^{-1}) of CNFs/PANI/Au nanofibers can still achieve more than 82.8% of the initial capacitance (292.1 F g^{-1}) value at a lower current density of 2 A g^{-1}.

Apparently, the CNFs/PANI/Au nanofiber electrodes can endure a wide range of current density cycle tests, which is an ideal characteristic for nanofiber electrodes. The unusual heterostructure of CNFs/PANI/Au nanofiber electrodes contributes to their good cycling stability: (1) homogeneous Au NPs decorating CNFs/PANI nanofibers can provide excellent charge carriers between the CNFs and PANI components, which is beneficial for establishing interconnecting channels and can effectively promote electron transfer efficiency; (2) the CNFs/PANI/Au nanofiber electrodes also possess a similar ultra-long 1D nanostructure as the CNFs supports, which is effective for optimizing the contact interface and shortening the charge transfer path between Au NPs and PANI components; (3) these freestanding electrodes, which do not require adhesives, effectively eliminate dead volume, boosting charge transfer and ion exchange between the electrolyte and the active material. Therefore, the obtained freestanding CNFs/PANI/Au nanofiber electrodes possess a unique 3D network structure, enhanced specific capacitance, and optimized cycling stability, implying their potential for flexible electronic devices or integrated applications.

4. Conclusions

In this work, freestanding CNFs/PANI/Au nanofiber electrodes with adjustable atomic weights of Au NPs and PANI nanostructures were flexibly integrated *via* a facile hierarchical assembly process. For the CNFs/PANI/Au nanofiber electrodes, we emphasize two advantages from a novel perspective: 1) the binder-free and freestanding

Fig. 5 Schematic diagram of the proposed mechanistic model of charge transfer occurring at the CNFs/PANI/Au nanofibers.

electrodes with 3D network nanostructures offer a continuous conducting route to enhance the fast transport/collection of electrons and ions at the electrode/electrolyte interface; 2) the nanofiber electrodes construct an efficient charge transfer channel using Au NPs as a charge transfer bridge, supporting the efficient charge transfer at the heterojunction interface. The freestanding CNFs/PANI/Au nanofiber electrode presents a desirable specific capacitance of 1144.5 F g^{-1} at a current density of 0.5 A g^{-1} and exhibits long-term stability, with about 86.5% specific capacitance retention at 2 A g^{-1} of incipient capacitance after 5000 cycles. The outstanding capacitive properties of the CNFs/PANI/Au nanofibers were closely related to their optimized 3D network nanostructures, excellent charge transportation, and unique electrode preparation method without the use of conductive adhesives. This work presents a new approach for the future of charge storage devices that use freestanding and binder-free electrodes generated from heterojunction nanofibers.

Data availability

The data presented in this study are available in article.

Author contributions

Yan Bu performed the data curation, investigation, and writing of the original draft; Yunwei Zou and Ruibai Cang contributed to investigation, methodology, and validation; Xuejiao Zhou contributed to conceptualization, reviewing, editing and funding acquisition; Peng Yu contributed to supervision and validation; Mingyi Zhang contributed to supervision, resources, and project administration.

Conflicts of interest

There are no conflicts to declare.

Acknowledgements

References

1 B. Joshi, E. Samuel, Y. il Kim, A. L. Yarin, M. T. Swihart and S. S. Yoon, Review of recent progress in electrospinning-derived freestanding and binder-free electrodes for supercapacitors, *Coord. Chem. Rev.*, 2022, **460**, 214466–214486, DOI: **10.1016/j.ccr.2022.214466**.

2 Y. Liang, Z. Wei, H. E. Wang, M. Flores, R. Wang and X. Zhang, Flexible and freestanding PANI: PSS/CNF nanopaper electrodes with enhanced electrochemical performance for supercapacitors, *J. Power Sources*, 2022, **548**, 232071–232080, DOI: **10.1016/j.jpowsour.2022.232071**.

3 W. Yang, Y. X. Zhu, Z. F. Jia, L. He, L. Xu, J. S. Meng, M. Tahir, Z. X. Zhou, X. W. Wang and L. Q. Mai, Interwoven nanowire based on-chip asymmetric microsupercapacitor with high integrability, areal energy, and power density, *Adv. Energy Mater.*, 2020, **10**, 2001873, DOI: **10.1002/aenm.202001873**.

4 B. B. Sahoo, N. Kumar, H. S. Panda, B. Panigrahy, N. K. Sahoo, A. Soam, B. S. Mahanto and P. K. Sahoo, Self-assembled 3D graphene-based aerogel with Au nanoparticles as high-performance supercapacitor electrode, *J. Energy Storage*, 2021, **43**, 103157–103166, DOI: **10.1016/j.est.2021.103157**.

5 J. Zhu, Q. Zhang, L. Guo, Y. Zhao, R. Zhang, L. Liu and J. Yu, Highly flexible, freestanding supercapacitor electrodes based on hollow hierarchical porous carbon nanofibers bridged by carbon nanotubes, *Chem. Eng. J.*, 2022, **434**, 134662–134673, DOI: **10.1016/j.cej.2022.134662**.

6 K. S. Yao, C. C. Zhao, N. N. Sun, W. W. Lu, Y. Zhang, H. Y. Wang and J. J. Wang, Freestanding CuS nanowalls: ionic liquid-assisted synthesis and prominent catalytic performance for the decomposition of ammonium perchlorate, *CrystEngComm*, 2017, **19**, 5048–5057, DOI: **10.1039/c7ce01119a**.

7 J. Cherusseri, K. S. Kumar, D. Pandey, E. Barrios and J. Thomas, Vertically aligned graphene-carbon fiber hybrid electrodes with superlong cycling stability for flexible supercapacitors, *Small*, 2019, **15**, 1902606, DOI: **10.1002/smll.201902606**.

8 J. Wang, Y. Ma, J. Liu, L. Zhu, X. Wu and X. Huang, Facile and controllable in-situ nitridation of polyaniline electrode for high-performance flexible all-solid-state supercapacitors, *J. Colloid Interface Sci.*, 2022, **620**, 399–406, DOI: **10.1016/j.jcis.2022.04.038**.

9 L. W. Hu, D. Xiang, Y. Gan, L. Y. Wen, X. W. Lv, M. L. Hu, Y. T. Xin and Z. R. Hou, Construction of N-doped nickel sulfide nanosheets via PANI as a nitrogen donor for superior electrocatalytic water splitting, *CrystEngComm*, 2023, **25**, 5021–5028, DOI: **10.1039/d3ce00555k**.

10 F. J. Miao, C. L. Shao, X. H. Li, K. X. Wang, N. Lu and Y. C. Liu, Freestanding hierarchically porous carbon framework decorated by polyaniline as binder-free electrodes for high performance supercapacitors, *J. Power Sources*, 2016, **329**, 516–524, DOI: **10.1016/j.jpowsour.2016.08.111**.

11 X. Lang, L. Zhang, T. Fujita, Y. Ding and M. Chen, Three-dimensional bicontinuous nanoporous Au/polyaniline hybrid films for high-performance electrochemical supercapacitors, *J. Power Sources*, 2012, **197**, 325–329, DOI: **10.1016/j.jpowsour.2011.09.006**.

12 H. Wang and Y. Xie, Hydrogen bond enforced polyaniline grown on activated carbon fibers substrate for wearable bracelet supercapacitor, *J. Energy Storage*, 2022, **52**, 105042–105054, DOI: **10.1016/j.est.2022.105042**.

13 J. Stejskal, D. Hlavatá, P. Holler, M. Trchová, J. Prokeš and I. Sapurina, Polyaniline prepared in the presence of various acids: a conductivity study, *Polym. Int.*, 2004, **53**, 294–300, DOI: **10.1002/pi.1406**.

14 Y. Jung, K. R. Pyun, J. K. Min, H. Yoon, M. Lee, B. W. Kim, J. Lee and S. H. Ko, An Ag-Au-PANI core-shell nanowire network for visible-to-infrared data encryption and supercapacitor applications, *J. Mater. Chem. A*, 2023, **11**, 7264–7275, DOI: **10.1039/d3ta00426k**.

15 J. Xu, J. Ding, X. Zhou, Y. Zhang, W. Zhu, Z. Liu, S. Ge, N. Yuan, S. Fang and R. H. Baughman, Enhanced rate performance of flexible and stretchable linear supercapacitors based on polyaniline@Au@carbon nanotube with ultrafast axial electron transport, *J. Power Sources*, 2017, **340**, 302–308, DOI: **10.1016/j.jpowsour.2016.11.085**.

16 Z. Çıplak, A. Yıldız and N. Yıldız, Green preparation of ternary reduced graphene oxide-au@polyaniline nanocomposite for supercapacitor application, *J. Energy Storage*, 2020, **32**, 101846–101857, DOI: **10.1016/j.est.2020.101846**.

17 K. N. Chaudhari, S. Chaudhari and J. S. Yu, Synthesis and supercapacitor performance of Au-nanoparticle decorated MWCNT, *J. Electroanal. Chem.*, 2016, **761**, 98–105, DOI: **10.1016/j.jelechem.2015.12.020**.

18 W. J. Cui, W. S. Lu, Y. K. Zhang, G. H. Lin, T. X. Wei and L. Jiang, Gold nanoparticle ink suitable for electric-conductive pattern fabrication using in ink-jet printing technology, *Colloids Surf., A*, 2010, **358**, 35–41, DOI: **10.1016/j.colsurfa.2010.01.023**.

19 A. K. Yagati, S. G. Chavan, C. Baek, D. Lee, M. H. Lee and J. Min, RGO-PANI composite Au microelectrodes for sensitive ECIS analysis of human gastric (MKN-1) cancer cells, *Bioelectrochemistry*, 2023, **150**, 108347–108357, DOI: **10.1016/j.bioelechem.2022.108347**.

20 L. Lin, M. Li, P. Li, C. Ye, H. Zhuang, S. Weng and F. Chen, Simultaneous determination of dopamine and uric acid based on electrocatalytic oxidation of Cu_2O-Au and polyaniline nanocomposites, *Microchem. J.*, 2024, **196**, 109602–109613, DOI: **10.1016/j.microc.2023.109602**.

21 L. Sun, H. Jing, S. Zhou, W. Tan, X. Ren, M. Zhang, X. Sun, H. Wang, T. Murayama and C. Qi, Manipulation of the electronic state of Au to boost the catalytic efficiency of Au/polyaniline by doping engineering, *Mol. Catal.*, 2024, **557**, 113963–113975, DOI: **10.1016/j.mcat.2024.113963**.

22 F. J. Miao, C. L. Shao, X. H. Li, K. X. Wang, N. Lu and Y. C. Liu, Three-dimensional freestanding hierarchically porous carbon materials as binder-free electrodes for supercapacitors: High capacitive property and long-term cycling stability, *J. Mater. Chem. A*, 2016, **4**, 5623–5631, DOI: **10.1039/c6ta00830e**.

23 Y. Zhou, Y. Zhu, B. Xu and X. Zhang, High electroactive material loading on a carbon nanotube/carbon nanofiber as an advanced free-standing electrode for asymmetric supercapacitors, *Chem. Commun.*, 2019, **55**, 4083–4086, DOI: **10.1039/c9cc01277j**.

24 E. Saeb and K. Asadpour-Zeynali, Facile synthesis of TiO_2@PANI@Au nanocomposite as an electrochemical sensor for determination of hydrazine, *Microchem. J.*, 2021, **160**, 105603, DOI: **10.1016/j.microc.2020.105603**.

25 S. Ur Rahman, P. Röse, M. Surati, A. U. H. A. Shah, U. Krewer and S. Bilal, 3D polyaniline nanofibers anchored on carbon paper for high-performance and light-weight supercapacitors, *Polymer*, 2020, **12**, 1–17, DOI: **10.3390/polym12112705**.

26 L. Wang, X. Wang, J. Ouyang, Y. Guo, W. Xiong, L. Zhao, M. Li, Z. Hua, Z. Li, K. Du, C. Zhou and Y. Luo, Construction of polyaniline/MnO_2 core-shell nanocomposites in carbonized wood tracheids for high-performance all-solid-state asymmetric supercapacitors, *Appl. Surf. Sci.*, 2023, **612**, 155821–155830, DOI: **10.1016/j.apsusc.2022.155821**.

27 Z. Q. Niu, P. S. Luan, Q. Shao, H. B. Dong, J. Z. Li, J. Chen, D. Zhao, L. Cai, W. Y. Zhou, X. D. Chen and S. S. Xia, A "skeleton/skin" strategy for preparing ultrathin free-standing single-walled carbon nanotube/polyaniline films for high performance supercapacitor electrodes, *Energy Environ. Sci.*, 2012, **5**, 8726–8733, DOI: **10.1039/C2EE22042C**.

28 S. Chen, Y. Zhang, D. Tian, Q. You, M. Zhong, C. Hu and J. Chen, Polyaniline combining with ultrathin manganese dioxide nanosheets on carbon nanofibers as effective binder-free supercapacitor electrode, *Electrochim. Acta*, 2023, **450**, 142275–142285, DOI: **10.1016/j.electacta.2023.142275**.

29 J. Zhu, Q. Zhang, H. Chen, R. Zhang, L. Liu and J. Yu, Setaria viridis-inspired electrode with polyaniline decorated on porous heteroatom-doped carbon nanofibers for flexible supercapacitors, *ACS Appl. Mater. Interfaces*, 2020, **12**, 43634–43645, DOI: **10.1021/acsami.0c10933**.

30 S. Liu, K. Wan, C. Zhang and T. Liu, Polyaniline-decorated 3D carbon porous network with excellent electrolyte wettability and high energy density for supercapacitors, *Compos. Commun.*, 2021, **24**, 100610–100616, DOI: **10.1016/j.coco.2020.100610**.

31 M. Liu, X. Li, C. Shao, C. Han, Y. Liu, X. Li, X. Ma, F. Chen and Y. Liu, Synchronous-ultrahigh conductive-reactive N-atoms doping strategy of carbon nanofibers networks for high-performance flexible energy storage, *Energy Storage Mater.*, 2022, **44**, 250–262, DOI: **10.1016/j.ensm.2021.10.025**.

32 F. Xie, H. Zhu, Y. Qu, J. Hu, H. Tan, K. Wang and L. Sun, Promoted OH– adsorption and electron-transfer kinetics by electrospinning mono-disperse $NiCo_2S_4$ nanocrystals within porous CNFs for solid asymmetric supercapacitors, *J. Colloid Interface Sci.*, 2024, **657**, 63–74, DOI: **10.1016/j.jcis.2023.11.103**.

33 D. Lv, D. Yin, Y. Yang, H. Shao, D. Li, T. Wang, Q. Ma, F. Li, W. Yu, C. Han and X. Dong, Self-supporting multi-channel Janus carbon fibers: A new strategy to achieve an efficient bifunctional electrocatalyst for overall water splitting, *J. Colloid Interface Sci.*, 2024, **663**, 270–279, DOI: **10.1016/j.jcis.2024.02.162**.

34 L. Li, X. Zhang, Z. Zhang, M. Zhang, L. Cong, Y. Pan and S. Lin, A bismuth oxide nanosheet-coated electrospun carbon nanofiber film: A free-standing negative electrode for flexible asymmetric supercapacitors, *J. Mater. Chem. A*, 2016, **4**, 16635–16644, DOI: **10.1039/c6ta06755g**.

35 M. Zhang, C. Shao, X. Li, P. Zhang, Y. Sun, C. Su, X. Zhang, J. Ren and Y. Liu, Carbon-modified $BiVO_4$ microtubes

embedded with Ag nanoparticles have high photocatalytic activity under visible light, *Nanoscale*, 2012, **4**, 7501–7508, DOI: **10.1039/c2nr32213g**.

36 X. J. Zhou, Y. Wang, Y. Wang, M. Y. Zhang, H. Gao and X. T. Zhang, Superior uniform carbon nanofibers@g-C$_3$N$_4$ core-shell nanostructures embedded by Au nanoparticles for high-efficiency photocatalyst, *J. Hazard. Mater.*, 2020, **388**, 121759–121770, DOI: **10.1016/j.jhazmat.2019.121759**.

37 F. J. Miao, C. L. Shao, X. H. Li, K. X. Wang, N. Lu and Y. C. Liu, Electrospun Carbon Nanofibers/Carbon Nanotubes/Polyaniline Ternary Composites with Enhanced Electrochemical Performance for Flexible Solid-State Supercapacitors, *ACS Sustainable Chem. Eng.*, 2016, **4**, 1689–1696, DOI: **10.1021/acssuschemeng.5b01631**.

38 X. B. Wei, C. L. Shao, X. H. Li, N. Lu, K. X. Wang, Z. Y. Zhang and Y. C. Liu, Facile in situ synthesis of plasmonic nanoparticles-decorated g-C$_3$N$_4$/TiO$_2$ heterojunction nanofibers and comparison study of their photosynergistic effects for efficient photocatalytic H$_2$ evolution, *Nanoscale*, 2016, **8**, 11034–11043, DOI: **10.1039/C6NR01491G**.

39 Z. Y. Zhang, C. L. Shao, P. Zou, P. Zhang, M. Y. Zhang, J. B. Mu, Z. C. Guo, X. H. Li, C. H. Wang and Y. C. Liu, In situ assembly of well-dispersed gold nanoparticles on electrospun silica nanotubes for catalytic reduction of 4-nitrophenol, *Chem. Commun.*, 2011, **47**, 3906–3908, DOI: **10.1039/c0cc05693f**.

40 Z. Y. Zhang, C. L. Shao, Y. Y. Sun, J. B. Mu, M. Y. Zhang, P. Zhang, Z. C. Guo, P. P. Liang, C. H. Wang and Y. C. Liu, Tubular nanocomposite catalysts based on size-controlled and highly dispersed silver nanoparticles assembled on electrospun silica nanotubes for catalytic reduction of 4-nitrophenol, *J. Mater. Chem.*, 2012, **22**, 1387, DOI: **10.1039/c1jm13421c**.

41 Y. Li, S. Ye, J. Lin, Y. Song, X. Wu, J. Zhang, C. Shao, Z. Su, H. Sun and D. S. Seferos, A pore-forming strategy toward porous carbon-based substrates for high performance flexible lithium metal full batteries, *Energy Environ. Mater.*, 2023, **6**, 1–9, DOI: **10.1002/eem2.12368**.

42 A. Atta, M. M. Abdelhamied, D. Essam, M. Shaban, A. H. Alshammari and M. Rabia, Structural and physical properties of polyaniline/silver oxide/silver nanocomposite electrode for supercapacitor applications, *Int. J. Energy Res.*, 2022, **46**, 6702–6710, DOI: **10.1002/er.7608**.

43 M. Zhang, A. Nautiyal, H. Du, Z. Wei, X. Zhang and R. Wang, Electropolymerization of polyaniline as high-performance binder free electrodes for flexible supercapacitor, *Electrochim. Acta*, 2021, **376**, 138037–138049, DOI: **10.1016/j.electacta.2021.138037**.

44 F. J. Miao, C. L. Shao, X. H. Li, N. Lu, K. X. Wang, X. Zhang and Y. C. Liu, Polyaniline-coated electrospun carbon nanofibers with high mass loading and enhanced capacitive performance as freestanding electrodes for flexible solid-state supercapacitors, *Energy*, 2016, **95**, 233–241, DOI: **10.1016/j.energy.2015.12.013**.

45 Z. Çıplak and N. Yıldız, Polyaniline-Au nanocomposite as electrode material for supercapacitor applications, *Synth. Met.*, 2019, **256**, 2–11, DOI: **10.1016/j.synthmet.2019.116150**.

46 N. Wang, G. Han, H. Song, Y. Xiao, Y. Li, Y. Zhang and H. Wang, Integrated flexible supercapacitor based on poly (3, 4-ethylene dioxythiophene) deposited on Au/porous polypropylene film/Au, *J. Power Sources*, 2018, **395**, 228–236, DOI: **10.1016/j.jpowsour.2018.05.074**.

47 A. Zada, Y. Qu, S. Ali, N. Sun, H. Lu, R. Yan, X. Zhang and L. Jing, Improved visible-light activities for degrading pollutants on TiO$_2$/g-C$_3$N$_4$ nanocomposites by decorating SPR Au nanoparticles and 2,4-dichlorophenol decomposition path, *J. Hazard. Mater.*, 2018, **342**, 715–723, DOI: **10.1016/j.jhazmat.2017.09.005**.

48 X. Zhang, C. L. Shao, X. H. Li, N. Lu, K. X. Wang, F. J. Miao and Y. C. Liu, In$_2$S$_3$/carbon nanofibers/Au ternary synergetic system: Hierarchical assembly and enhanced visible-light photocatalytic activity, *J. Hazard. Mater.*, 2015, **283**, 599–607, DOI: **10.1016/j.jhazmat.2014.10.005**.

49 S. M. T. Kazmi, Z. Zahoor, N. T. Yusra, M. H. Bhatti, M. F. Afsar, F. Sher, H. Ur Rashid and M. A. Rafiq, Diode parameters extraction and study of space charge limited current in (Ag, Au)/CoS$_2$ Schottky diodes, *Phys. B*, 2023, **670**, 415400–415406, DOI: **10.1016/j.physb.2023.415400**.

50 P. Zhang, C. L. Shao, X. H. Li, M. Y. Zhang, X. Zhang, C. Y. Su, N. Lu, K. X. Wang and Y. C. Liu, An electron-rich free-standing carbon@Au core-shell nanofiber network as a highly active and recyclable catalyst for the reduction of 4-nitrophenol, *Phys. Chem. Chem. Phys.*, 2013, **15**, 10453–10458, DOI: **10.1039/c3cp50917f**.

51 H. G. Yun, X. J. Zhou, H. R. Zhu and M. Y. Zhang, One-dimensional zinc-manganate oxide hollow nanostructures with enhanced supercapacitor performance, *J. Colloid Interface Sci.*, 2021, **585**, 138–147, DOI: **10.1016/j.jcis.2020.11.060**.

52 S. Anand, M. W. Ahmad, A. K. Ali Al Saidi, D. J. Yang and A. Choudhury, Polyaniline nanofiber decorated carbon nanofiber hybrid mat for flexible electrochemical supercapacitor, *Mater. Chem. Phys.*, 2020, **254**, 123480–123490, DOI: **10.1016/j.matchemphys.2020.123480**.

53 P. Taravati Ahmad, B. Jaleh, S. Khazalpour, R. Gharehbaghi and R. S. Varma, Electrochemical fabrication of rGO/PANI-Au-γMnO$_2$ nanocomposites as supercapacitor electrode materials, *J. Mater. Sci.: Mater. Electron.*, 2021, **32**, 3038–3053, DOI: **10.1007/s10854-020-05054-3**.

54 J. Zhu, C. L. Shao, X. H. Li, C. H. Han, S. Yang, J. Ma, X. H. Li and Y. C. Liu, Immobilization of ZnO/polyaniline heterojunction on electrospun polyacrylonitrile nanofibers and enhanced photocatalytic activity, *Mater. Chem. Phys.*, 2018, **214**, 507–515, DOI: **10.1016/j.matchemphys.2018.04.053**.

55 W. Yu, F. Mo, J. Guo, Y. Yang, Y. Jin and Y. Fu, Ultrasensitive microRNA photoelectric assay based on a mimosa-like CdS-NiS/Au schottky junction, *Anal. Chem.*, 2023, **95**, 12097–12103, DOI: **10.1021/acs.analchem.3c02153**.